Research Square

Preprints are preliminary reports that have not undergone peer review.
They should not be considered conclusive, used to inform clinical practice,
or referenced by the media as validated information.

Inter-ictal Event Dynamics of Tonic-clonic Seizures

Farah Deeba

f.deeba@duet.ac.bd

Dhaka University of Engineering & Technology

F. A. Jibon

Dhaka University of Engineering & Technology

Hasna Hena

Dhaka University of Engineering & Technology

Peter A. Robinson

The University of Sydney

Research Article

Keywords:

Posted Date: November 20th, 2026

DOI: https://doi.org/10.21203/rs.3.rs-11566252/v1

License: This work is licensed under a Creative Commons Attribution 4.0 International License.
Read Full License

Additional Declarations: No competing interests reported.

Inter-ictal Event Dynamics of Tonic-clonic Seizures

F. Deeba*
Dhaka University of Engineering and Technology, Gazipur 1700, Bangladesh and
Dhaka University of Engineering and Technology, Gazipur 1700, Bangladesh

F. A. Jibon
Department of Computer Science and Engineering,
International University of Business Agriculture and Technology, Dhaka, Bangladesh

H. Hena
Department of Mathematics, Dhaka University of Engineering and Technology, Gazipur 1700, Bangladesh

P. A. Robinson
School of Physics, University of Sydney, NSW 2006, Australia
(Dated: November 3, 2026)

The evolution of the interictal dynamics during generalized tonic-clonic seizure and their proximity to seizure events are investigated by employing a neural field model of the corticothalamic system. Interictal events are modeled as transient changes near the seizure threshold in connection strength between the cortex and thalamus, which drive the system toward seizure oscillations.As the connection strength increases, distinct oscillations emerge: (i) low-frequency delta spikes when the duration or amplitude of the changing profile of the connection strength is too small; (ii) ~ 18 Hz saddle-cycle oscillations for a moderate duration and amplitude of the changing profile; and finally, (iii) typical ~ 10 Hz seizure activity when the system crosses the seizure threshold well. The morphology and spectral characteristics of these oscillation events depend on the magnitude, duration, and gain of the excursion. The transition between the events reflects a progression from well-established delta spikes to the saddle cycle oscillations to seizure states. Machine learning analysis of patient data from the CHB-MIT scalp EEG database, confirms the presence of 18 Hz oscillations prior to seizures, supporting the model's predictions. Using these tracks and dependencies the proximity to seizure can be estimated and controlled.

* f.deeba@duet.ac.bd; farah.ju35@gmail.com

I. INTRODUCTION

Tonic-clonic seizures are among the most common generalized epileptic seizures [1]. They are characterized by typical ~ 10 Hz wave oscillations with tonic and clonic phases. The tonic phase is marked by an initial increase in muscle tone, while the clonic phase, which often follows, is characterized by bilateral symmetric jerking of the extremities [2]. These seizures typically last 1 to 3 minutes and show distinguishable preictal and post-ictal electroencephalograms (EEG).

The markedly different preictal characteristics of tonic-clonic seizures have led to an optimistic approach to predict upcoming episodes [3–9]. Epileptiform events, such as spikes and sharp waves, often appear on the EEG between seizures. The frequency of these interictal events is widely used to predict seizures [3–18]. However, many studies report mismatches between this conventional approach and actual seizure occurrences, where observing spikes or sharp waves alone often generates false alarms or misses real alarms [3, 4, 19].

This paper begins with the conjecture that a detailed investigation of interictal events before seizures could provide better insight into the preictal-to-ictal transition. Deeba *et al.* [20] investigated the detail dynamics during the ictal phase of tonic-clonic seizure. It was seen that if the connection strength between the different populations of the cortex and thalamus increases and crosses a certain threshold value of seizures, the brain undergoes seizure-like oscillations. The wave properties and dynamics depend largely on changing profile (viz. rate of change, duration of change, etc.) of the connection strength. A thorough investigation also revealed the existence of unstable 18 Hz saddle-cycle oscillations before the beginning of proper 10 Hz seizure oscillations for certain cases with a high rate of change of the connection strength. Other studies [21] also find the existence of the saddle-cycle during early seizure oscillations. As all the 18 Hz oscillations are seen in the beginning of ictal state, especially, when the system is still near to the modeled seizure threshold limit, it can be hypothesised that the 18 Hz are connected with inter-ictal phase as well. Therefore, an expanded investigation, similar to the approach in [20], but in interictal state will let us understand the impact of the 18 Hz saddle-cycle during interictal phase. Therefore, this study aims to examine the impact of the presence of these 18 Hz oscillations in preictal states and their correlation with the onset of seizures. In addition, since the ~ 18 Hz saddle-cycle oscillations appear a few seconds before the 10 Hz oscillations or spikes [20], using these oscillations as an additional indication for the inter-ictal phase might improve the accuracy of the prediction and might allow a few extra seconds for medication.

In this paper, interictal events are modeled based on the hypothesis that they are the result of transient parameter excursions beyond the seizure threshold, specifically through temporal variations in corticothalamic connection strength [22]. A widely used neural field model of the corticothalamic system, which has previously unified and reproduced various observed features of brain activities such as evoked response potentials [23], activity spectra [24], and neurological disorders such as seizures [22, 25] and Parkinson's disease, is used to study the dynamics of interictal and ictal events during generalized tonic-clonic seizures. A detailed analysis of the dynamics of interictal events, their evolution, and their dependence on physiological parameters is performed. The existence and characteristics of ~ 18 Hz saddle-cycle oscillations are thoroughly studied, and machine learning analysis of patient data from the CHB-MIT scalp EEG database is run to test and confirm the predictions of the model.

The outline of this paper is as follows. The Methodology section describes the corticothalamic neural field model, the temporal variation function, and the numerical methods. The Modeling Outcomes section analyzes the evolution of interictal event morphology, spectral characteristics, and their proximity to ictal oscillations. The Data Analysis section details the machine learning analysis of CHB-MIT scalp EEG data to confirm the presence of $\sim$ 18 Hz oscillations before seizures. Finally, the Discussion summarizes the outcomes and explores their potential applications.

II. METHODOLOGY

This section contains a brief description of the corticothalamic neural field model used, together with the temporal variation function of the corticothalamic coupling strength [20, 22, 25]. Further details of the model can be found in [26–28].

A. Corticothalamic Field Model

To investigate the interictal dynamics of tonic-clonic seizures, the neural field model of the corticothalamic system seen in Fig. 1 is used. In this study, the model of [22] is used but in different parametric regimes suitable for studying the interictal events.

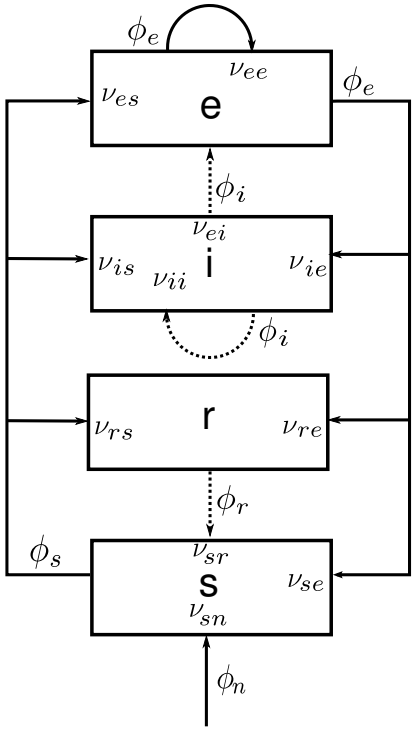


FIG. 1: Schematic diagram of the corticothalamic model system. Depicted neural populations are cortical excitatory (e), inhibitory (i), thalamic reticular (r), thalamic relay (s), and n = external inputs. The parameter ν_{ab} represents the connection strengths to population a from population b. Dashed lines represent inhibitory connections.

The neural populations in this study are represented as: e = excitatory cortical; i = inhibitory cortical; s =

thalamic relay neurons; r = thalamic reticular nucleus; and n = external inputs. The local mean cell-body potential V_a, the mean firing rate in the cell-body Q_a, and the propagating axonal fields ϕ_a are the dynamical variables within each neural population a. The firing rates Q_a, which are functions of position $\mathbf{r}$ and time t, are related to potentials V_a by the response function:

$$Q_a(\mathbf{r}, t) = S[V_a(\mathbf{r}, t)], \tag{1}$$

where S is a smooth sigmoidal function that increases from 0 to $Q_{\max}$ as V_a increases from $-\infty$ to ∞, with

$$S(V_a) = \frac{Q_{\max}}{1 + \exp[-\pi(V_a - \theta)/\sigma\sqrt{3}]}, \tag{2}$$

where θ is the mean neural firing threshold, σ is the standard deviation of this threshold, and $Q_{\max}$ is the maximum firing rate [26, 27].

The firing rates Q_a produce propagating axonal fields ϕ_a in each neural population that approximately obey the damped wave equation

$$D_a\phi_a(\mathbf{r}, t) = Q_a(\mathbf{r}, t), \tag{3}$$

where D_a is the spatiotemporal differential operator, expressed as

$$D_a = \frac{1}{\gamma_a^2}\frac{\partial^2}{\partial t^2} + \frac{2}{\gamma_a}\frac{\partial}{\partial t} + 1 - r_a^2\nabla^2, \tag{4}$$

where $\gamma_a = v_a/r_a$ is the damping rate, r_a and v_a are the characteristic range and conduction velocity of axons of type a, and ∇^2 is the Laplacian operator. Equation 4 incorporates time delays within populations; however, the smallness of r_i, r_s, and r_r allows us to set $\gamma_a \simeq \infty$ except for $a = e$.

After the propagation and filtering of the postsynaptic potentials through the dendritic tree, the cell-body potential V_a are generated and then summed. For excitatory and inhibitory neurons within the cortex, V_a is approximated via the second-order delay-differential equation [27]

$$D_\alpha V_a(\mathbf{r}, t) = \nu_{ae}\phi_e(\mathbf{r}, t) + \nu_{ai}\phi_i(\mathbf{r}, t) + \nu_{as}\phi_s(\mathbf{r}, t - t_0/2), \tag{5}$$

where $a = e, i$ and the temporal differential operator is given by

$$D_\alpha = \frac{1}{\alpha\beta}\frac{d^2}{dt^2} + \left(\frac{1}{\alpha} + \frac{1}{\beta}\right)\frac{d}{dt} + 1. \tag{6}$$

The quantities α and β in Eq. (6) are the inverse decay and rise times, respectively, of the cell-body potential produced by an impulse at a dendritic synapse. The input from the thalamus to the cortex is delayed by a propagation time $t_0/2$. The inputs from the cortex are time delayed within the specific and reticular nuclei of the thalamus, so

$$\begin{aligned} D_\alpha V_a(\mathbf{r}, t) = \nu_{ae}\phi_e(\mathbf{r}, t - t_0/2) + \nu_{as}\phi_s(\mathbf{r}, t) \\ +\nu_{ar}\phi_r(\mathbf{r}, t) + \nu_{an}\phi_n(\mathbf{r}, t), \end{aligned} \tag{7}$$

where $a = s, r$. The connection strengths are given by $\nu_{ab} = N_{ab}s_{ab}$, where N_{ab} is the mean number of synapses to neurons of type a from type b and s_{ab} is the strength of the response in neurons a to a unit signal from neurons of type b. The final term on the right-hand side of Eq. (7) describes inputs from outside the corticothalamic system. Among the 16 possible connections between the four neural populations, only 10 connections shown in Fig. 1 are included to simplify the model [27].

The random intracortical connectivity and the number of connections between populations are also assumed proportional to the number of synapses [29], which provides $N_{ib} = N_{eb}$ for all b, so $\nu_{ee} = \nu_{ie}$, $\nu_{ei} = \nu_{ii}$ and $\nu_{es} = \nu_{is}$ [30]. The global (spatially invariant) corticothalamic steady states, which corresponds to the normal brain activity [27, 31], is obtained by setting all spatial and temporal derivatives in Eqs $(2) - (7)$ to zero.

B. Parameter Excursions

The propagation and rise of synchronous neuronal oscillations occur through the coupling mechanisms between different neuronal populations. Previous studies have shown that an increase in the coupling strength between different neuronal populations drives the system into a limit cycle from a stable steady state via bifurcation, which causes periodic seizure-like oscillations [20, 22, 25, 26]. Before reaching the stable limit cycle attractor, the system was also seen to undergo via a small unstable saddle cycle attractor, which leads to small seizure-like oscillations [20]. These small oscillations shows similar pattern to the interictal events [20], which are brief reoccurring synchronous oscillations often observed between two consecutive seizure attacks. These recurring oscillations do not drive the system to the seizure state, however, leave significant traces with repeating patterns observable in the EEG recordings, which often foreshadow seizures. Therefore, we start from the ansatz that each interictal event corresponds to a brief excursion beyond the seizure threshold but far below the limit cycle attractor. In this paper, we intend to explore the dynamical evolution of the interictal events with the increasing physiological properties.

The time-dependent parabolic ramp [22], which is used to model the excursion of corticothalamic coupling strength ν_{se} is given by

TABLE I: Nominal parameters of the neural field model from [26]

Parameter	Value	Unit	Meaning
ν_{ee}	1.2	mV s	Excitatory corticocortical connectivity
ν_{ei}	-1.8	mV s	Inhibitory corticocortical connectivity
ν_{es}	1.4	mV s	Specific thalamic to cortical connectivity
ν_{re}	0.2	mV s	Cortical to thalamic reticular connectivity
ν_{rs}	0.2	mV s	Specific to reticular thalamic connectivity
ν_{se}	1.0	mV s	Cortical to specific thalamic connectivity
ν_{sr}	-1.0	mV s	Reticular to specific thalamic connectivity
$\nu_{sn}\phi_n$	2.0	mV	Subthalamic input
$Q_{\max}$	250	s^{-1}	Maximum firing rate
θ	15	mV	Mean neuronal threshold
σ	6	mV	Threshold standard deviation
γ_e	100	s^{-1}	Damping rate
α	60	s^{-1}	Decay rate of membrane potential
β	240	s^{-1}	Rise rate of membrane potential
t_0	80	ms	Corticothalamic return time (complete loop)
t_1	100	s	Center of the ramp rise
t_2	200	s	Center of the ramp fall
$\nu_{\max}$	1.2	mV s	Maximum value of ν_{se}
ν_0	0.8	mV s	Minimum value of ν_{se}
Δ	10	s	Characteristic rise time

$$\nu_{se}(t) = \nu_\theta + 4(\nu_{\max} - \nu_\theta)\left[\frac{(t-t_1)(t_2-t)}{(t_2-t_1)^2}\right], \tag{8}$$

where $\nu_{se}(t) \geq \nu_0$ and ν_0 otherwise, ν_θ is the seizure threshold, which is 0.8 mV s for tonic-clonic seizure for the parameters in Table I [20], t_1 is the time at which ν_{se} crosses ν_θ during ramping up, t_2 is the time at which ν_{se} crosses ν_θ during ramping down, $\nu_{\max}$ is the maximum value of ν_{se}. Figure 2 shows ν_{se} vs. t showing $\nu_{\max}$, ν_0, ν_θ, t_1, and t_2.

The parameters in Table I are used as initial parameters, which are taken from [26] and [20]. To initialize the system in the vicinity of the bifurcation threshold, the ramp-up of ν_{se} starts from $\nu_0 = 0.9$ mV s, for every simulation. The $\nu_{\max}$ ranges from 1.00 mV to 1.45 mV s.

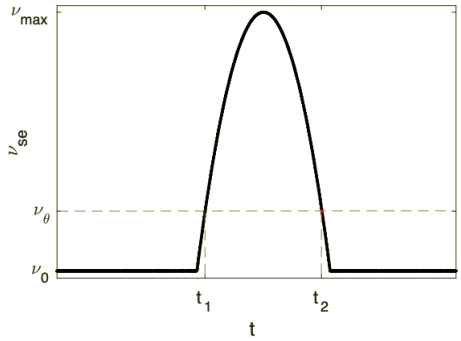


FIG. 2: Temporal profile of ν_{se} varying from ν_0 to $\nu_{\max}$ and back, crossing the threshold ν_θ at times t_1 and t_2.

C. Numerical Methods

To study the inter-ictal events, a detailed analytical exploration of the modeling data has been performed, along with a brief exploration of the available free scalp data to visually compare the outcomes. Therefore, this study is divided into two segments: analytic exploration and machine learning analysis.

1. Analytic Exploration

For the analytic exploration, neural field software *NFTsim* [32] is used to solve Eqs (1) – (7) numerically for the spatially uniform case in which the ∇^2 term in Eq. (4) is zero, in order to consider generalized activity and seizures. To vary ν_{se} temporally, Eq. (8) is used. Because there is a propagation time delay $t_0/2$ between the different neural populations present in Eqs (6) and (7), this involves solving ordinary delay differential equations. *NFTsim* uses a fourth-order Runge-Kutta integration to solve these equations, with an integration time step of 10^{-4} s, and stores time histories of the delay terms over an interval of $t_0/2$ into the past.

Simulations are started close to a corticothalamic steady state with a low firing rate because the normal brain operates close to stable fixed points [26, 27, 33, 34]. Gradually the connection strengths are increased to the point where the system exhibits fully developed limit cycle seizure oscillations, after which it returns to the initial starting steady state point. However, for the presence of the delay time $t_0/2$, these initial steady-state conditions are specified to apply for times $-t_0/2 < t \leqslant 0$.

A constant input $\nu_{sn}\phi_n = 2$ mV is used and no external noise is applied in the simulations. The total simulations are 100 s long with a temporal variation ranging from $1 - 10$. The output time series is recorded every 0.5 ms. For all simulations, the default parameters are shown in Table I unless otherwise specified. For spectral analysis, a fast Fourier transform with a Hanning window of 6000 data points 0.6 s long, an overlap of 500 points, and a sampling rate of 10000 Hz is employed.

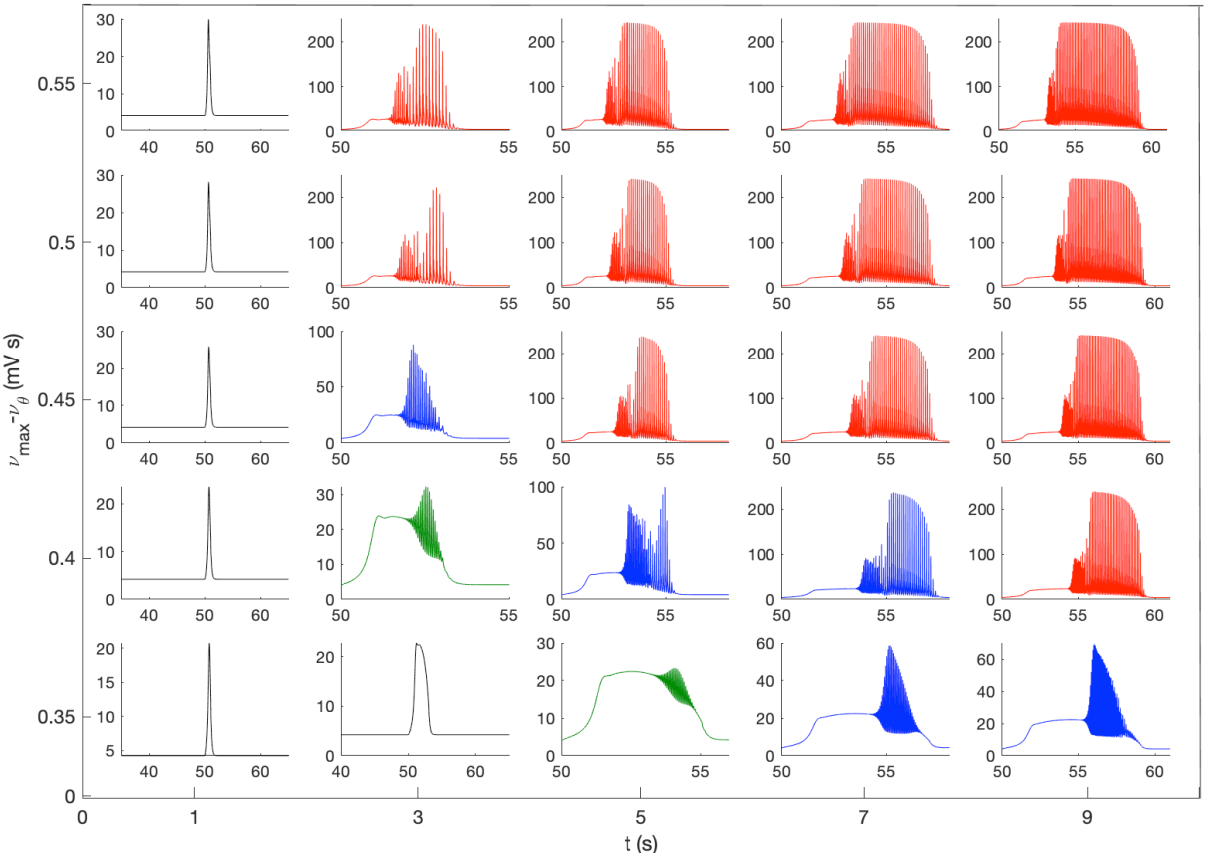


FIG. 3: Time series of ϕ_e vs. $t_2 - t_1$ and $\nu_{\max} - \nu_0$ ranges from 1 to 10 s and 0.35 to 0.55 mV s, respectively. Spikes are shown in black, where small sharp waves with green, developed saddle-cycles with blue and seizure oscillations in black, respectively.

2. *Machine Learning Analysis*

For the machine learning analysis, we explore the Scalp EEG Database of [35], which contains EEG recordings of 22 pediatric subjects with intractable seizures. An international 10-20 system of electrode positions and EEG nomenclature was used and the signals were sampled at 256 samples per second with 16 bit resolution. The data set includes a total of 182 annotated seizure events.

To process and visualize the data, the Python libraries, including Matplotlib and NumPy, have been used. The EEG recordings are segmented into 6-second intervals, and a band-pass filter is applied to isolate frequencies in bands like alpha, beta, and gamma. For the saddle-cycle filtering, we only consider the frequencies range from 18-20 Hz. The reason behind this extremely narrow filtering was to distinguish the impact of the saddle-cycle ($18Hz$) from the others.A rigorous analysis of the data would provide a broader picture of the interictal events. However, as this paper is primarily a model–outcome-based analysis and we employ ML only to compare our outcomes, we constrain ourselves to the simplest analysis.

III. INTERICTAL DYNAMICS EVOLUTION

In this section, we observe the impact of the transient excursion of the corticothalamic connection strength on the dynamics of interictal events. First, we explore the possible morphologies of the events and relate them to the physiological parameters of the excursion. Then we analyze the general and spectral characteristics of each type of interictal and ictal event in detail.

A. General Characteristics

To see the impact of the transient excursion, we first analyze the dependence of the wave morphology of the oscillations on the physiological parameters of the excursion. First, we vary $\nu_{\max}$ from 1.00 mV s to 1.45 mV s and Δt from 1 s to 10 s. Figure 3 shows the time series of ϕ_e vs. $t_2 - t_1$ and $\nu_{\max} - \nu_0$ ranging from 1 to 10 s and 0.35 to 0.55 mV s, respectively. The observed oscillation patterns in Fig. 3 are:

1. Single spike-like oscillations (black oscillations in Fig. 3) are observed for a very low $t_2 - t_1$, regardless of any range of $\nu_{\max}$. These spikes resemble the clinically observed interictal spikes [4]. For a very brief $t_2 - t_1$, the amplitude of the spikes increases with increasing $\nu_{\max}$. The number of spikes increases with the increase of $t_2 - t_1$ and gradually convert into the sharp wave oscillations. The increase in the number of spikes preceding seizures, reported in many clinical studies [4], is in line with the outcome observed in this region of the parameter space.

2. With increasing $t_2 - t_1$ and $\nu_{\max}$, small damped sharp wave oscillations appear (green oscillations in Fig. 3). A number of clinical studies also found the appearance of sharp waves prior seizure [4]. A detailed spectral and phase space analysis shows that with increasing $\nu_{\max}$ and $t_2 - t_1$, the system gradually starts to move towards the unstable saddle-cycle attractor; however, since $\nu_{\max}$ and $t_2 - t_1$ are still too small to reach the attractor, the system returns to steady state before reaching it. Therefore, we might also define these oscillations as undeveloped saddle-cycle oscillations.

3. With further increase of Δt, fully developed $\sim$ 18 Hz saddle-cycle oscillations (blue oscillations in Fig. 3) are seen, whose amplitude increases with $\nu_{\max}$ and $t_2 - t_1$. These saddle-cycle oscillations look like typical sharp wave oscillations but with a frequency of $\sim$ 18 Hz. With increasing $\nu_{\max}$ and $t_2 - t_1$, small-amplitude $\sim$ 10 Hz seizure oscillations start to accompany the saddle-cycle oscillation.

4. Finally, for enough $\nu_{\max}$ and $t_2 - t_1$, fully developed $\sim$ 10 Hz seizure oscillations (red oscillations in Fig. 3) appear, when the system reaches the stable limit cycle attractor. The amplitude of the seizure oscillations also increases with $\nu_{\max}$ and $t_2 - t_1$.

Therefore, if we want to map the evolution of the wave morphology of the system from a non-seizure stable state to an oscillating seizure state, we might get a map with spike $\rightarrow$ ringing-spike or underdeveloped saddle-cycle $\rightarrow$ fully developed unstable saddle-cycle $\rightarrow$ seizure oscillation track. This morphological evolution of the dynamic character-

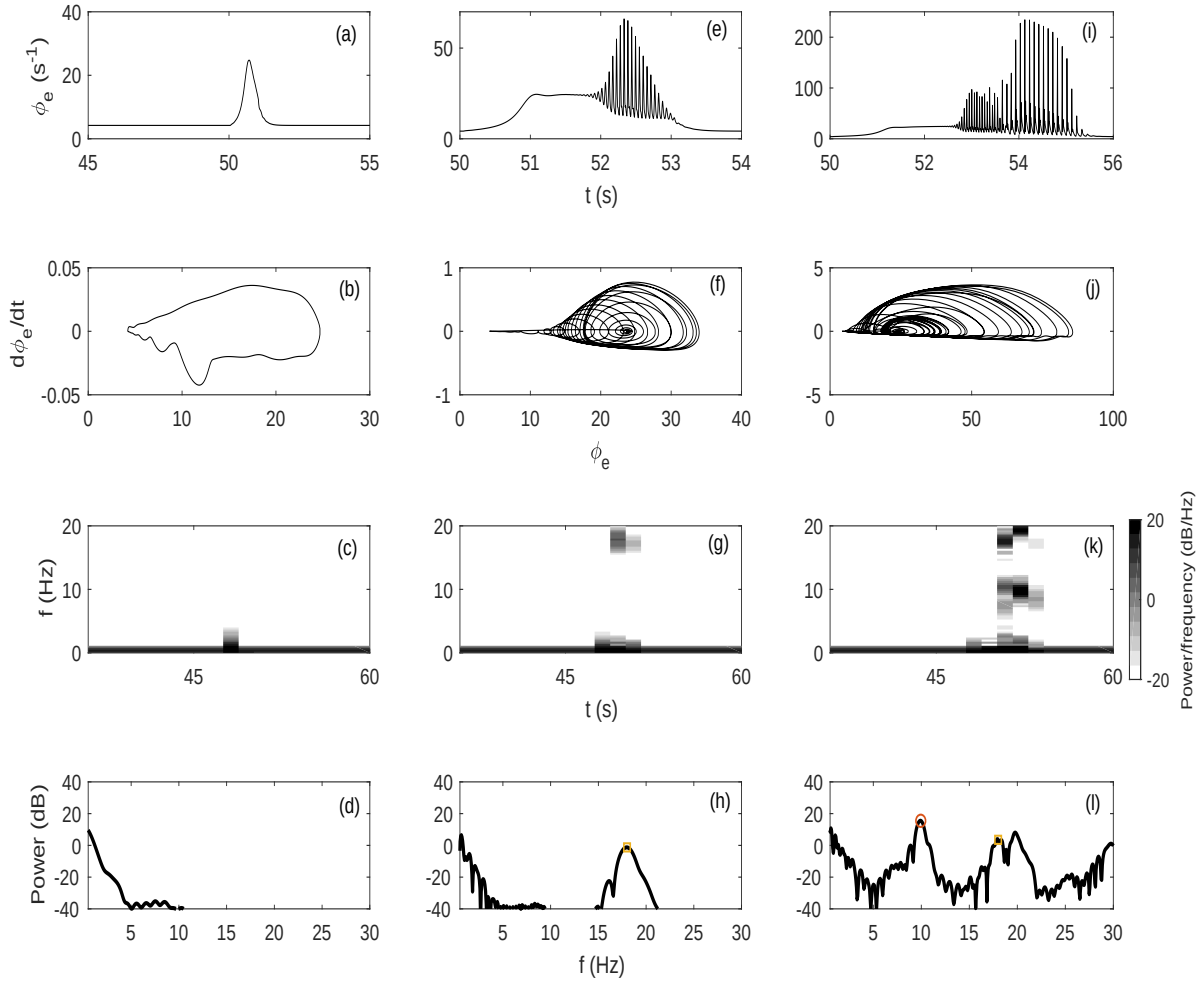


FIG. 4: Detailed dynamics of interictal oscillations seen in Fig. 3 for different $\nu_{\max} - \nu_0$ and $t_2 - t_1$ in different regions with rest of the fixed parameters of Table I. Frames (a)-(d) show the dynamical analysis of the spike, seen at $t_2 - t_1 = 1$ s and $\nu_{\max} - \nu_0 = 0.525$ mV s: (a) ϕ_e vs. t; (b) Phase space diagram; (c) Dynamic spectrum; and (d) power spectrum. Frames (e)-(h) show the dynamical analysis of saddle-cycle oscillation, seen at $t_2 - t_1 = 5$ s and $\nu_{\max} - \nu_0 = 0.45$ mV s: (e) ϕ_e vs. t; (f) Phase space diagram; (g) Dynamic spectrum; and (h) Power spectrum. Finally, frames (i)-(l) show the ~ 10 Hz seizure oscillation seen at $t_2 - t_1 = 5$ s: (i) ϕ_e vs. t; (j) Phase space diagram; (k) Dynamic spectrum and (l) Power spectrum.

istics of waves is observed for the increase of either $\nu_{\max}$ and $t_2 - t_1$ or of both. In the following sections, we discuss the detailed characteristics of each wave morphology.

B. Dynamical Characteristics

The detailed dynamical characteristics of distinct wave patterns observed in Fig. 3 are shown in Fig. 4. Panels 4(a)–4(d) show the dynamics of spikes depicted in black colour in Fig. 3. Figure 4(a) shows a zoomed version of the time series of ϕ_e vs. t for $\nu_{\max} = 1.325$ $\nu_{\max} - \nu_0 = 0.525$ mV s and $t_2 - t_1 = 1$. These morphology and characteristics of these single 3 Hz Spikes resemble the commonly observed clinical spikes [4, 22]. Figure 4(b) shows the corresponding phase space diagram showing a single excursion with a small spike over time. Figure 4(c) and (d) shows the corresponding dynamic and power spectrum, respectively. In both diagram, a low frequency delta $0 - 3Hz$ oscillation is seen.

Figures 4(e)–(h) show the saddle-cycle oscillation for $\nu_{\max} = 1.25$ mV s or $\nu_{\max} - \nu_0 = 0.45$ mV s and $t_2 - t_1 = 7$ s. These are the oscillations highlighted with blue in Fig. 3. Figure 4(e) shows a zoomed version of the time series of ϕ_e vs. t, while Fig. 4(f) shows the corresponding phase-space diagram. It is seen that the system spirals out to the unstable saddle-cycle attractor with increasing ν_{se} and gradually returns to the stable fixed point with decreasing ν_{se}. The corresponding dynamic and power spectrum are shown in 4(g) and (h), respectively, where prominent $\sim$ 18Hz peaks are seen. These saddle-cycle oscillations are also seen in recent studies [20, 21] just prior to the start of the seizure oscillations with a high rate of change of the connection strength [22]. Our present study confirms that saddle-cycle oscillations not only accompany seizure oscillations but also appear individually during inter-ictal periods for the cases with high $\nu_{\max}$ or low $t_2 - t_2$. The existence of individual saddle-cycle oscillations during the inter-ictal period leads to the possibility of using them as seizure indicators along with the spikes.

Finally, 4 (i)–(l) show a characteristic tonic-clonic seizure oscillation for $\nu_{\max} = 1.325$ mV s and $t_2 - t_1 = 5$ s. Figure 4(i) shows a zoomed version of the time series of ϕ_e vs. t. Figure 4(j) shows the corresponding phase-space diagram, where the system is seen to reach the limit cycle attractor with increasing ν_{se} and returns to the steady state with decreasing ν_{se}. Figures 4(k) and (l) show the corresponding dynamic spectrum and power spectrum, respectively. The dynamic spectrum shows a 10 Hz harmonic band, but with a bent edge towards the inside. Fig. 4(l) shows characteristic seizure peaks of $\sim$ 10 Hz [20]. A 18 Hz peak is also visible with 10 Hz which explains the bent of the frequency band towards the inside of Fig. 4(k). Now this band bending was also reported in many cases in [20].

C. Morphological Evolution

A close observation of fig. 4 suggests a spike $\rightarrow$ saddle-cycle $\rightarrow$ spike-wave dynamic evolution track prior to a seizure attack. We hypothesize that the oscillation patterns depend on the rate of change of ν_{max} over time. In this section, a quantitative assumption of the dependence of the interictal oscillation patterns on the gain of the system is presented to design a generalized seizure prediction mechanism.

A previous study [20] of the ictal dynamics of tonic-clonic seizure showed that a characteristic time is required to exhibit fully developed limit cycle oscillations and the properties of this characteristic time and seizure oscillations depend on the maximum connection strength. To understand the dynamics during inter-ictal states properly, we also need to understand their dependencies on similar physiological parameters like characteristic time and maximum

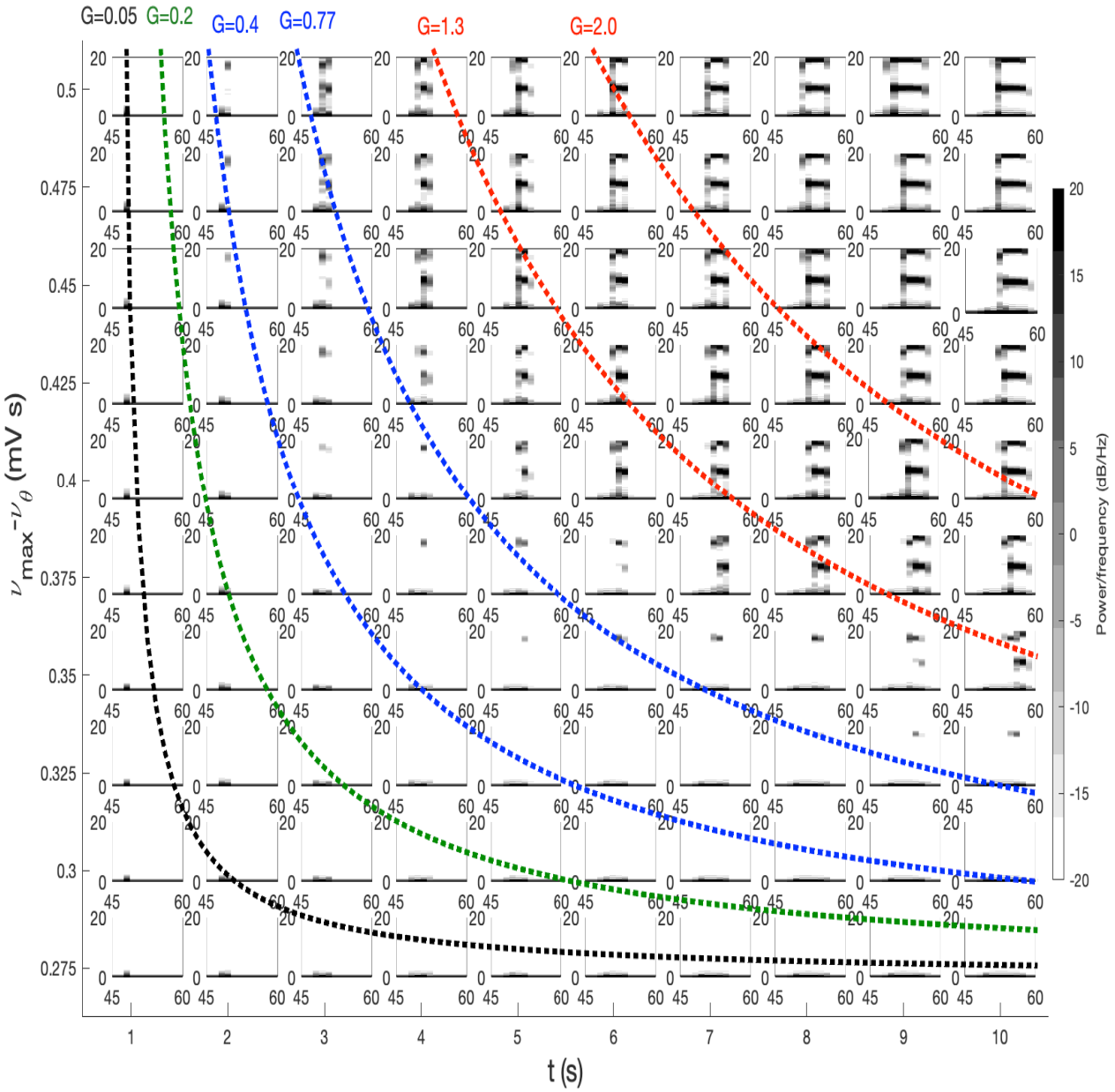


FIG. 5: Dynamical spectra of ϕ_e for $t_2 - t_1$ and $\nu_{\max} - \nu_\theta$ from 0.25 to 0.55 mV s. Dashed traces show curves of constant gain as labeled at the top. The color bar shows the power of the oscillations.

connection strength. Previous figures suggest a dependency of dynamic profiles on the rate of change or the gain of the profile of $\nu_{\max}$.

As in previous work [22], we approximate the amplitude dynamics near the threshold depends on ν_{se} and Δt, we

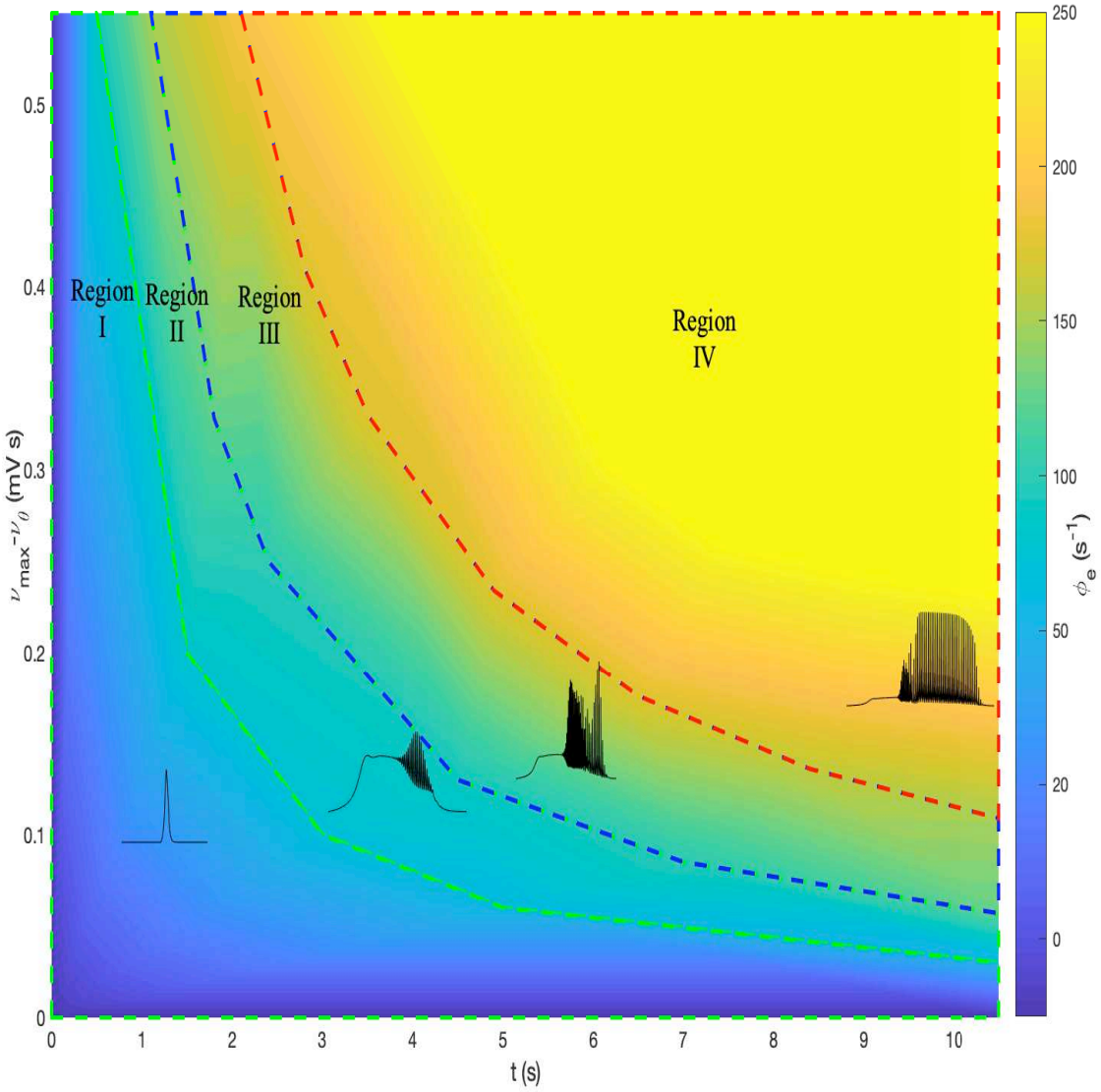
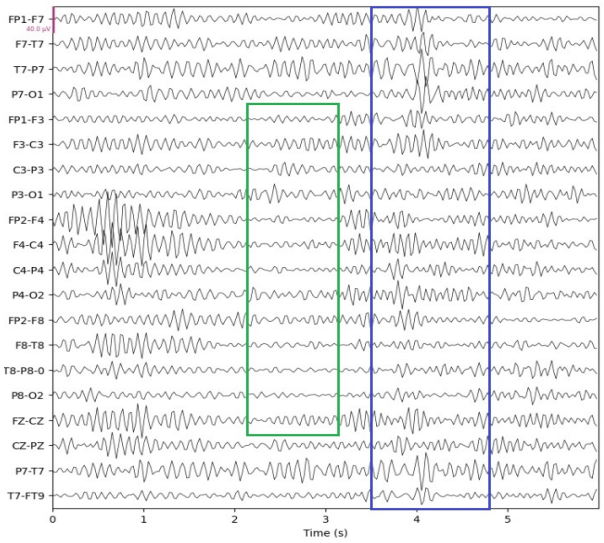


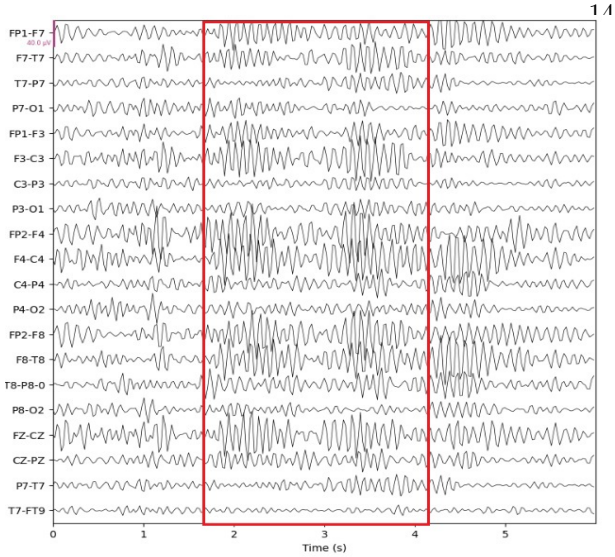
FIG. 6: Main dynamical regimes vs. $t_2 - t_1$ and $\nu_{\max} - \nu_\theta$, based on Fig. 3 with approximate boundaries shown. Region I is the spike-dominating zone (separated by green dashed line), Region II (region between green and blue dashed line) is the zone where spikes followed by small ringing and weak undeveloped saddle-cycle oscillations are seen; Region III (region between blue and red dashed line) is the saddle-cycle oscillations zone, and finally, Region IV (region at the left of the red dashed line) is the ictal zone where seizure oscillations are seen. The color bar shows the maximum amplitude of ϕ_e.

write the amplitude $A(t)$ for $\nu(t) \approx \nu_\theta$ at $t = t_1$ as:

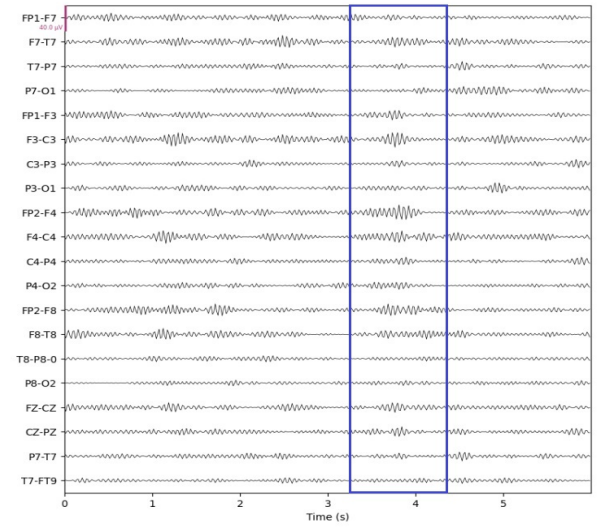
$$\frac{\mathrm{d}A}{\mathrm{d}t} \approx C\left[\nu(t) - \nu_\theta\right] A, \tag{9}$$



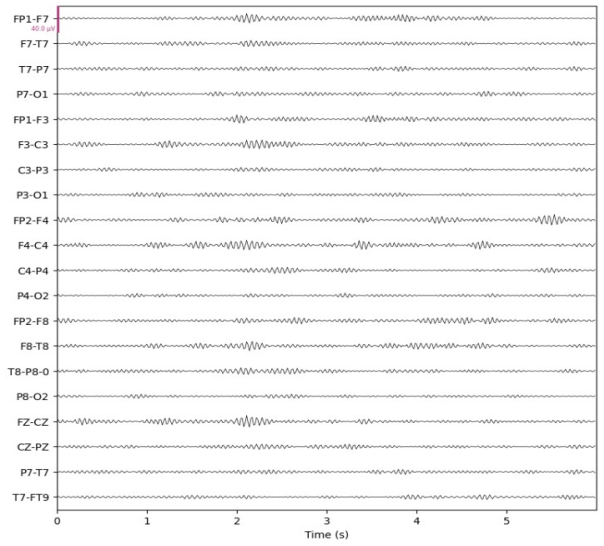
(a)



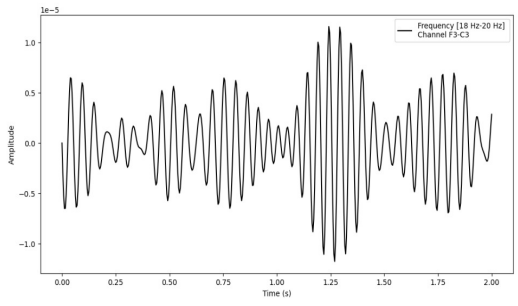
(b)



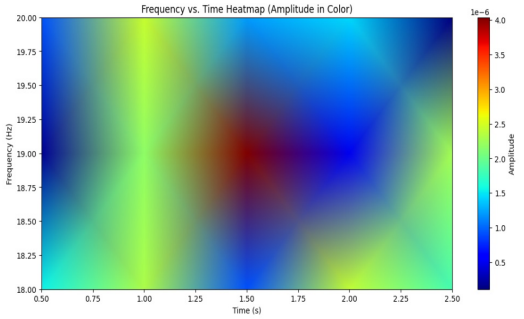
(c)



(d)



(e)



(f)

FIG. 7: Data analysis of patient no. chb15 from the CHB-MIT Scalp EEG data set. (a) shows unfiltered EEG time series from 264 s – 270 s exhibiting spikes (highlighted with green box), saddle-cycle like oscillations (highlighted with blue box); (b) shows consecutive unfiltered EEG time series from 264 s to 270 s exhibiting seizure oscillations (highlighted with red box); (c) shows respective $18 - -20$ Hz filtered time series of panel(a) with the highlighted 18 Hz wave packet; (d) shows respective $18 - -20$ Hz filtered time series of panel(d); (e) shows a zoomed segment of channel F3-C3 showing a 18 Hz wave packet of panel (c), and, finally (f) shows the corresponding spectrogram.

where C is a constant, and $\nu(t)$ is the instantaneous value of ν_{se}. Because ν_{se} only varies with time t, the time dependence of ν_{se} can be approximated as $\nu(t) - \nu_\theta \approx c\, q(t) \geqslant 0$ about the threshold; where

$$q(t) = 4(\nu_{\max} - \nu_\theta)\left[\frac{(t-t_1)(t_2-t)}{(t_2-t_1)^2}\right],$$

which yields

$$A(t) = A_\theta \exp\left[C\int_{t_1}^{t_2} q(t)dt\right], \tag{10}$$

with $c \approx C$, and $A(t) = A_\theta$ at $t = t_\theta$, $t_2 = t$, and $t_1 = t_\theta$. The range of the integral is taken in such a way that $t_2 - t_1 = \delta t$, where δt is the infinitesimal time interval between t_1 and t_2. The total gain $G = \ln(A/A_\theta)$ while above threshold, is then

$$G = C\int_{t_1}^{t_2} q(t)dt = \frac{2}{3}C(\nu_{\max} - \nu_\theta)(t_2 - t_1); \tag{11}$$

which depends only on $\nu_{\max} - \nu_\theta$ and $t_2 - t_1$ via their product. One can argue that any morphological shape change would primarily affect only the constant C, for example, on dimensional grounds.

To see the dependence of the wave morphology on the gain, G, we plot the dynamical spectrum of corresponding ϕ_e in the $t_2 - t_1$ and $\nu_{\max} - \nu_0$ space with the predictor of the gain distributions in Eq. 11. Figure 5 shows the dynamical spectral evolution of ϕ_e in $t_2 - t_1$ vs. $\nu_{\max} - \nu_0$ region with $t_2 - t_1$ ranges from 1 to 10 s and $\nu_{\max} - \nu_0$ ranges from 0.25 to 0.55 mV s, with gains $G = 0.2$ to $G = 2$.

The region, represented by the black curve, represents the area dominated by the delta spikes. The spikes are seen mainly for gain $G < 0.2$. The green dotted area for the gain $G = 0.2$ is the area where small undeveloped saddle-cycle oscillations dominate. This area extends up to the blue dotted area with $G = 0.4$, from where more fully developed saddle-cycle oscillations begin to appear. With time, seizure oscillations begin to accompany saddle-cycle oscillations. For $G = 0.77$, we see some 10 Hz seizure oscillations with the 18 Hz saddle-cycles. The regions for the gain $G < 0.77$, the system mostly exhibits fully developed typical 10 Hz limit cycle oscillations.

Figure 6 shows a gradual morphological transition from the interictal states to the ictal state depicting the dominant wave patterns in each region. Four major morphological regions are separated depending on the observation of fig. 6, which are:

1. Region I, a spike-dominant region with a small $\Delta t(\nu_{\max} - \nu_\theta)$. As much as the system moves toward the green dotted line, the shape of the spikes becomes distorted.

2. Region II, a mixed region with delta spikes observed in Region I but often followed by small ringings and undeveloped 18 Hz saddle-cycle oscillations. As much as the system moves toward the blue dotted line, more prominent and well-developed saddle-cycle oscillations start to appear, and as much as the system moves toward the green dotted line, more unperturbed delta spikes are seen.

3. Region III, is the region covers the area between the blue and red dotted lines. This region is dominated by the $\sim$ 18 Hz saddle-cycle oscillation. The more the system moves towards the red curve, the more $\sim$ 10 Hz seizure-like oscillations start to appear with the saddle-cycle oscillation.

4. Finally, Region VI is the region where the system moves to the seizure state and fully developed $\sim$ 10 Hz limit-cycle seizure oscillations are seen.

This parametric excursion map has no physical existence; however, it might be a key-tool to understand the present physiological state of the patient. The improvement of treatment can also be tracked by observing the wave morphological changes in the brain and comparing them with the map.

IV. DATA ANALYSIS

In this section, we analyze the wave morphology and their spectral properties of a random recording from the CHB-MIT Scalp EEG Database [35] to compare our model prediction to the real-life data. We again emphasise, we perform this analysis only to confirm the existence of $\sim$ 18 Hz saddle-cycle oscillations as all other wave forms are stablish and observed in many prior theoretical and clinical studies [4]. Extensive analysis of these data can obviously be possible; however, that is out of scope in our present study.

Figure 7 shows the data analysis of a random patient from the CHB-MIT Scalp EEG data set. Figure 7 (a) shows unfiltered interictal EEG time series of a 16-year-old male patient (file no. chb15) for the recording time range 264 s – 270 s. Here, spike-like oscillations (highlighted with a green box) and saddle-cycle-like oscillations (blue box) are seen. Both the profiles of the spikes and saddle-cycle oscillations resemble our computational outcomes shown in previous figures. Figure 7(b) shows the next consecutive time series in which a seizure attack is seen at 272 s, which is right after the appearance of the saddle-cycle wave packets

To observe more clearly the existence of the saddle-cycle oscillation, we applied a bandpass filtering of $18 - 20$ Hz in both Figs. 7(a) and (b), which are shown in Figs. 7(c) and (d). Several wave packets resembling the shape of the predicted saddle-cycle oscillations of Fig. 3 are seen in inter-ictal states in Fig. 7(c). The subsequent time series (Fig. 7(b)) analysis with the bandpass filter in Fig. 7(d) shows the presence of saddle-cycle oscillations in the initial states of the seizure attack as well. This outcome coincides with the prediction of [20]. Figure 7(e) shows a zoomed segment of Fig. 7(c). An series of sharp wave packets are visible in this figure. Finally, Fig. 7(f) shows the corresponding frequency spectrum, where a prominent $\sim$ 18 Hz oscillation is present.

We found the existence of a similar $\sim$ 18 Hz wave packet prior to the seizure attack in all samples in the data set. As this paper focuses on the modeling approach, we limit ourselves to these primary investigations. A detailed data fitting will give more detailed insight into the situation.

V. DISCUSSION

In this study, we employed a multiple analytical approach to investigate the interictal dynamics of tonic-clonic seizures in detail. This study provides a unified description of the dynamical transitions of oscillation patterns from the steady state to the seizure state. A generalized investigation is essential to understand the interictal dynamics properly as well as use them to predict the upcoming seizure attack. The predictions of this study, especially the prediction of the existence of the saddle-cycle oscillation in the interictal spectrum, not only will answer some of the mismatches between the upcoming seizure verses the seizure prediction of the existing algorithms, but will also open a new way to develop a more accurate seizure prediction mechanisms.

A neural field model of the corticothalamic system [26, 27] have been used to study the dynamics of interictal and ictal oscillation of tonic-clonic seizures, together with their dependence on the temporal profile of an assumed underlying corticothalamic connection strength excursion. We have modeled interictal events and seizures together as being caused by parameter excursions above the seizure threshold of the corticothalamic connection strength, and studied the progression of interictal events—specifically, the transition from spikes to seizures—through the emergence of 18 Hz saddle oscillations. Three major observed event dynamics are:

1. Delta spikes, which are seen for too small $t_2 - t_1$ and high $\nu_{\max} - \nu_\theta$ or large $t_2 - t_1$ and low $\nu_{\max} - \nu_\theta$. These spikes resemble the well known spikes observed in many clinical studies prior to seizure. The amplitude of these delta spikes increases with increasing $\nu_{\max}$.

2. 18 Hz saddle-cycle oscillations for medium $t_2 - t_1$ and high $\nu_{\max} - \nu_\theta$. These oscillation serves as an intermediate unstable $\sim$ 18 Hz saddle-cycle oscillations are seen, whose amplitude and duration increase with increasing $\nu_{\max}$ and $t_2 - t_1$, respectively.

3. For sufficiently high $t_2 - t_1$ and $\nu_{\max} - \nu_\theta$, $\sim$ 10 Hz limit-cycle seizure oscillations dominate. The amplitude and duration of seizure oscillations also increase with increasing $\nu_{\max}$ and $t_2 - t_1$, respectively.

In particular, for all types of oscillations, the number of oscillations seen increases with $t_2 - t_1$ and their amplitude increases with $\nu_{\max} - \nu_\theta$. The spikes and saddle-cycle oscillations are both found to be accompanied by the following types of oscillations with increasing $t_2 - t_1$ and $\nu_{\max} - \nu_\theta$. An imaginary parametric area showing the schematic dominant regions of the oscillation patterns is also drawn, which might be helpful to distinguish the personalisation of the situation of the patients.

If other connection strengths than the corticothalamic one were varied, ν_{se}, qualitative predictions could be made successfully using the present outcomes because they will exhibit similar dynamics due to the universality properties of the Hopf bifurcation [26].

The delta spikes found in the first region are seen in a number of previous studies and are also used as a very well-accepted seizure prediction tool [4]. However, the second interictal oscillation profile, which is the saddle-cycle oscillations, is only reported by very few as an accompanying oscillation with the seizure oscillations [20, 21]. Claiming

the saddle-cycles as interictal dynamics as well as a good tool to predict upcoming seizure is a new concept. To support the idea, we used ML to analyze current real patient data from CHB-MIT [35]. An intense analysis through ML also confirms the existence of saddle-cycle oscillations prior to a seizure attack.

In conclusion, the above results clarify the relationships between interictal events and tonic-clonic seizures and show that interictal events like spikes and saddle cycles can arise from a single cause and can both be used as a seizure prediction tool. A further illustration of the present work might lead to possible implications for informing clinical interventions, and seizure control strategies.

We thank [35] for providing the CHB-MIT scalp data set.

Acknowledgements

We thank [35] for providing the CHB-MIT scalp data set.

DECLARATIONS

- Funding: This work was done under the research project entitled "Quantitative Modeling of Neurological Disorders", supported by the University Grants Commission of Bangladesh (UGC) at Dhaka University of Engineering and Technology, Gazipur.
- Conflict of interest/Competing interests: No known conflict of interest.
- Ethics approval: Not applicable.
- Consent for publication: Yes.
- Data availability: Will be provided upon request.
- Materials availability: Will be provided upon request.

[1] J. Engel, T. A. Pedley, Epilepsy: A comprehensive textbook, Vol. 1, Lippincott-Raven, Philadelphia, 1997.

[2] T. R. Browne, G. L. Holmes, Handbook of epilepsy, Lippincott Williams & Wilkins, Philadelphia, 2000.

[3] K. Staley, J. L. Hellier, F. E. Dudek, Do interictal spikes drive epileptogenesis?, The Neuroscientist 11 (4) (2005) 272–276.

[4] P. J. Karoly, D. R. Freestone, R. Boston, D. B. Grayden, D. Himes, K. Leyde, U. Seneviratne, S. Berkovic, T. O'Brien, M. J. Cook, Interictal spikes and epileptic seizures: their relationship and underlying rhythmicity, Brain 139 (4) (2016) 1066–1078.

[5] J. Gotman, J. R. Ives, P. Gloor, Automatic recognition of inter-ictal epileptic activity in prolonged eeg recordings, Electroencephalography and Clinical Neurophysiology 46 (5) (1979) 510–520.

[6] J. Gotman, Relationships between interictal spiking and seizures: human and experimental evidence, Canadian Journal of Neurological Sciences 18 (S4) (1991) 573–576.

[7] F. Wendling, A. Hernandez, J.-J. Bellanger, P. Chauvel, F. Bartolomei, Interictal to ictal transition in human temporal lobe epilepsy: insights from a computational model of intracerebral eeg, Journal of Clinical Neurophysiology 22 (5) (2005) 343.

[8] F. H. Lopes da Silva, W. Blanes, S. N. Kalitzin, J. Parra, P. Suffczynski, D. N. Velis, Epilepsies as dynamical diseases of brain systems: basic models of the transition between normal and epileptic activity, Epilepsia 44 (2003) 72–83.

[9] K. Lehnertz, R. G. Andrzejak, J. Arnhold, T. Kreuz, F. Mormann, C. Rieke, G. Widman, C. E. Elger, Nonlinear eeg analysis in epilepsy: its possible use for interictal focus localization, seizure anticipation, and prevention, Journal of Clinical Neurophysiology 18 (3) (2001) 209–222.

[10] B. L. Ralston, The mechanism of transition of interictal spiking foci into ictal seizure discharges, Electroencephalography and Clinical Neurophysiology 10 (2) (1958) 217–232.

[11] B. L. Ralston, C. A. Papatheodorou, The mechanism of transition of interictal spiking foci into ictal seizure discharges part ii: Observations in man, Electroencephalography and Clinical Neurophysiology 12 (2) (1960) 297–304.

[12] J. Jacobs, P. LeVan, R. Chander, J. Hall, F. Dubeau, J. Gotman, Interictal high-frequency oscillations (80–500 hz) are an indicator of seizure onset areas independent of spikes in the human epileptic brain, Epilepsia 49 (11) (2008) 1893–1907.

[13] J. Engel, R. F. Ackermann, Interictal eeg spikes correlate with decreased, rather than increased, epileptogenicity in amygdaloid kindled rats., Brain Research (1980).

[14] N. Milligan, J. Oxley, A. Richens, Acute effects of intravenous phenytoin on the frequency of inter-ictal spikes in man., British Journal of Clinical Pharmacology 16 (3) (1983) 285–289.

[15] D. S. Goodin, M. J. Aminoff, Does the interictal eeg have a role in the diagnosis of epilepsy?, The Lancet 323 (8381) (1984) 837–839.

[16] C.-G. Bénar, D. W. Gross, Y. Wang, V. Petre, B. Pike, F. Dubeau, J. Gotman, The bold response to interictal epileptiform discharges, NeuroImage 17 (3) (2002) 1182–1192.

[17] G. E. Chatrian, C.-M. Shaw, H. Leffman, The significance of periodic lateralized epileptiform discharges in eeg: an electrographic, clinical and pathological study, Clinical Neurophysiology 17 (2) (1964) 177–193.

[18] B. Pohlmann-Eden, D. B. Hoch, J. I. Cochius, K. H. Chiappa, Periodic lateralized epileptiform discharges–a critical review, Journal of Clinical Neurophysiology 13 (6) (1996) 519–530.

[19] K. Maeda, N. Hosoda, H. Tsuboi, H. Naito, C. Kudo, J. Fukumoto, S. Fujita, N. Ichino, K. Osakabe, K. Sugimoto, S. Yamaguchi, N. Ishihara, The appearance of scalp high-frequency oscillations is associated with poor seizure control in pediatric epilepsy patients, Epilepsia Open 10 (2024) 107–119. doi:10.1002/epi4.13032.

[20] F. Deeba, P. Sanz-Leon, P. A. Robinson, Effects of the physiological parameter evolution on the dynamics of tonic-clonic seizure, PLoS One 15 (2020) e0230510.

[21] D. P. Yang, P. A. Robinson, Critical dynamics of hopf bifurcations in the corticothalamic system: Transitions from normal arousal states to epileptic seizures, Physical Review E 95 (4) (2017) 042410.

[22] F. Deeba, P. Sanz-Leon, P. A. Robinson, Unified dynamics of interictal events and absence seizures, Phys. Rev. E 100 (2019) 022407.

[23] C. J. Rennie, P. A. Robinson, J. J. Wright, Unified neurophysical model of eeg spectra and evoked potentials, Biological Cybernetics 86 (6) (2002) 457–471.

[24] S. C. O'Connor, P. A. Robinson, Spatially uniform and nonuniform analysis of electroencephalographic dynamics, with application to the topography of the alpha rhythm, Physical Review E 70 (1) (2004) 011911.

[25] F. Deeba, P. Sanz-Leon, P. A. Robinson, Dependence of absence seizure dynamics on physiological parameter evolution,

Journal of Theoretical Biology 454 (2018) 11–21.

[26] M. Breakspear, J. A. Roberts, J. R. Terry, S. Rodrigues, N. Mahant, P. A. Robinson, A unifying explanation of primary generalized seizures through nonlinear brain modeling and bifurcation analysis, Cerebral Cortex 16 (9) (2006) 1296–1313.

[27] P. A. Robinson, C. J. Rennie, D. L. Rowe, Dynamics of large-scale brain activity in normal arousal states and epileptic seizures, Physical Review E 65 (4) (2002) 041924.

[28] F. Marten, S. Rodrigues, O. Benjamin, M. P. Richardson, J. R. Terry, Onset of polyspike complexes in a mean-field model of human electroencephalography and its application to absence epilepsy, Philosophical Transactions of the Royal Society of London A 367 (1891) (2009) 1145–1161.

[29] D. T. J. Liley, P. J. Cadusch, J. J. Wright, A continuum theory of electro-cortical activity, Neurocomputing 26 (1999) 795–800.

[30] R. G. Abeysuriya, C. J. Rennie, P. A. Robinson, Physiologically based arousal state estimation and dynamics, Journal of Neuroscience Methods 253 (2015) 55–69.

[31] P. A. Robinson, C. J. Rennie, J. J. Wright, Propagation and stability of waves of electrical activity in the cerebral cortex, Physical Review E 56 (1) (1997) 826.

[32] P. Sanz-Leon, P. A. Robinson, S. A. Knock, P. M. Drysdale, R. G. Abeysuriya, P. K. Fung, C. J. Rennie, X. Zhao, NFTsim: Theory and simulation of multiscale neural field dynamics, PLoS Computational Biology 14 (8) (2018) e1006387.

[33] P. A. Robinson, C. J. Rennie, D. L. Rowe, S. C. O'Connor, E. Gordon, Multiscale brain modelling, Philosophical Transactions of the Royal Society B 360 (1457) (2005) 1043–1050.

[34] P. A. Robinson, C. J. Rennie, D. L. Rowe, S. C. O'Connor, Estimation of multiscale neurophysiologic parameters by electroencephalographic means, Human Brain Mapping 23 (1) (2004) 53–72.

[35] A. L. Goldberger, L. A. Amaral, L. Glass, J. M. Hausdorff, P. C. Ivanov, R. G. Mark, J. E. Mietus, G. B. Moody, C.-K. Peng, H. E. Stanley, Physiobank, physiotoolkit, and physionet: components of a new research resource for complex physiologic signals, circulation 101 (23) (2000) e215–e220.